Circular Bragg supermirror

Tom G. Mackay[a,b,*], **Akhlesh Lakhtakia**[b]
[a]University of Edinburgh, School of Mathematics and Maxwell Institute for Mathematical Sciences, Edinburgh EH9 3FD, Scotland, United Kingdom
[b]Pennsylvania State University, Department of Engineering Science and Mechanics, NanoMM–Nanoengineered Metamaterials Group, University Park, PA 16802, USA

Abstract. The helical nanowires of a chiral sculptured thin film (CSTF) were taken to be made from a weakly dissipative material while the void regions between nanowires were filled with an active material, and the planewave reflection/transmission characteristics were investigated numerically. The CSTF was found to simultaneously amplify left-circularly polarized incident light and attenuate right-circularly-polarized incident light, or vice versa, depending upon its structural handedness. This polarization-state-dependent attenuation and amplification phenomenon is sensitive to the direction of incidence and the thickness of the CSTF. Furthermore, the presence of both dissipative and active materials allows the high reflectance to exceed unity across a substantial proportion of the circular Bragg spectral regime for incident light of one circular polarization state but not of the other circular polarization state. That is, the CSTF functions as a circular Bragg supermirror for one, and only one, circular polarization state.

Keywords: Circular Bragg phenomenon, amplification, attenuation, chiral sculptured thin film.

*Tom G. Mackay, T.Mackay@ed.ac.uk

1 Introduction

By combining materials in a judicious manner, unusual and potentially useful optical properties may be realized.[1] In particular, theoretical studies in the past few years have revealed that exotic optical response characteristics can be exhibited by certain engineered composite materials arising from a combination of active and dissipative component materials. For example, a uniaxial dielectric material, in which plane waves traveling in one direction are amplified but plane waves traveling in another direction are attenuated, can be conceived via the homogenization of a random mixture of active and dissipative oriented spheroidal particles that are electrically small.[2] In a similar vein, a periodic multilayer comprising alternate active and dissipative layers may be optically equivalent to a birefringent material which allows arbitrary control over polarization states.[3] Also, the homogenization of a composite material with active and dissipative component materials can give rise to an isotropic chiral material that amplifies left-circularly polarized (LCP) light but attenuates right-circularly polarized (RCP) light (or vice versa).[4] Parenthetically, active component materials are also extensively used to combat intrinsic dissipation in a wide variety of metamaterials.[5–9]

A columnar thin film comprising both dissipative and active component materials can attenuate light of one linear polarization state but amplify light of the other linear polarization state.[10] Furthermore, the reflectance of an adequately thick periodic multilayer with a unit cell consisting of two different columnar thin films — each constructed from dissipative nanocolumn materials but with active materials filling the intercolumnar regions[11] — exceeds unity for s-polarized incident light but not for p-polarized incident light (or vice versa) in the Bragg regime.[12,13] This structure is referred to as a *Bragg supermirror* for the linear polarization state whose the reflectance exceeds unity, but not for the other linear polarization state.

In the present study, we theoretically explore the prospects for a chiral sculptured thin film (CSTF) to function as a Bragg supermirror for circularly polarized light. We note that engineered materials comprising helical structures have been proposed and investigated for a variety of electromagnetic purposes for over 150 years,[14–20] based on their ability to discriminate between LCP light and RCP light, and this area of research still remains active.[21–27] However, the prospect of supermirror behavior has not previously been investigated for such materials.

2 Constitutive parameters of infiltrated CSTF

Consider a CSTF of thickness L, whose helical nanowires are aligned parallel to the z axis. The periodically nonhomogeneous relative permittivity dyadic of the CSTF may be expressed as[20]

$$\underline{\underline{\varepsilon}}_{cstf}(z) = \underline{\underline{S}}_z\left(\frac{h\pi z}{\Omega}\right) \cdot \underline{\underline{S}}_y(\chi) \cdot \underline{\underline{\varepsilon}}_{ref} \cdot \underline{\underline{S}}_y^{-1}(\chi) \cdot \underline{\underline{S}}_z^{-1}\left(\frac{h\pi z}{\Omega}\right), \quad 0 < z < L, \tag{1}$$

where the local orthorhombic symmetry of the helical nanowires is characterized by the reference relative permittivity dyadic[28]

$$\underline{\underline{\varepsilon}}_{ref} = \varepsilon_a\, \mathbf{u}_z\mathbf{u}_z + \varepsilon_b\, \mathbf{u}_x\mathbf{u}_x + \varepsilon_c\, \mathbf{u}_y\mathbf{u}_y\,, \tag{2}$$

whereas the rotational nonhomogeneity and the rise of the helical nanowires along the z axis are captured by the dyadic functions

$$\underline{\underline{S}}_z(\zeta) = (\mathbf{u}_x\mathbf{u}_x + \mathbf{u}_y\mathbf{u}_y)\cos\zeta + (\mathbf{u}_y\mathbf{u}_x - \mathbf{u}_x\mathbf{u}_y)\sin\zeta + \mathbf{u}_z\mathbf{u}_z \tag{3}$$

and

$$\underline{\underline{S}}_y(\chi) = (\mathbf{u}_x\mathbf{u}_x + \mathbf{u}_z\mathbf{u}_z)\cos\chi + (\mathbf{u}_z\mathbf{u}_x - \mathbf{u}_x\mathbf{u}_z)\sin\chi + \mathbf{u}_y\mathbf{u}_y\,, \tag{4}$$

respectively. Here, the structural handedness parameter $h = 1$ for right handedness and $h = -1$ for left handedness, 2Ω is the structural period, χ is the rise angle of the helical nanowires, and ζ is the orientation angle with respect to the x axis in the xy plane. A schematic illustration of a single helical nanowire in a CSTF is provided in Fig. 1. The three unit vectors aligned with the Cartesian axes are denoted by $\mathbf{u}_x$, $\mathbf{u}_y$, and $\mathbf{u}_z$.

The relative permittivity scalars ε_a, ε_b, and ε_c were estimated using a homogenization procedure based on the Bruggeman formalism (and its inverse),[29–31] as follows. Helical nanowires occupy a proportion $f \in (0,1)$ of the CSTF's total volume; i.e., the volume fraction of the CSTF not occupied by nanowires is $1 - f$. Every helical nanowire is regarded as a string of highly elongated ellipsoidal inclusions wound end-to-end around the z axis.[20] The shape of each ellipsoidal inclusion is prescribed by the dyadic

$$\underline{\underline{U}} = \mathbf{u}_n\,\mathbf{u}_n + \gamma_\tau\,\mathbf{u}_\tau\,\mathbf{u}_\tau + \gamma_b\,\mathbf{u}_b\,\mathbf{u}_b, \tag{5}$$

wherein γ_τ and γ_b are positive-valued shape parameters, and the unit vectors

$$\left.\begin{aligned} \mathbf{u}_n &= -\mathbf{u}_x\,\sin\chi + \mathbf{u}_z\,\cos\chi\,, \\ \mathbf{u}_\tau &= \mathbf{u}_x\,\cos\chi + \mathbf{u}_z\,\sin\chi\,, \\ \mathbf{u}_b &= -\mathbf{u}_y \end{aligned}\right\}. \tag{6}$$

In order to impose an aciculate shape on the inclusions, the shape parameters are taken to satisfy $\gamma_b \gtrsim 1$ and $\gamma_\tau \gg 1$. Indeed, since increasing γ_τ beyond 10 does not give rise to significant effects for slender inclusions,[32] we fixed $\gamma_\tau = 15$.

The homogenization procedure involved three steps: First, the nanowires of CSTF were taken to be made from zirconium oxide. By means of the inverse Bruggeman homogenization formalism,[32] using experimental data on $\varepsilon_{a,b,c}$ at the free-space wavelength $\lambda_0 = 633$ nm,[33] the refractive index of the nanowire material was estimated to be 2.266 when $\chi = 37.105$ deg. The inverse Bruggeman formalism simultaneously yielded $\gamma_b = 2.535$ and $f = 0.430$. Second, the nanowires of the CSTF were taken to be impregnated with 0.2% v/v silver nanoparticles. By means of the Biot–Arago formula,[34] the refractive index of the nanowire material was revised as $2.261 + 0.009i$, after using the bulk refractive index of silver for $\lambda_0 = 633$ nm.[35] Third, the inter-nanowire void regions of the CSTF were modeled as filled with a mixture of rhodamine 800 and rhodamine 6G. Such a rhodamine mixture has a relative permittivity whose real part lies in the range $(1.8, 2.3)$ and whose imaginary part lies in the range $(-0.15, -0.02)$ over the 440–500-THz frequency range, depending upon the relative concentrations and the external pumping rate.[9] For definiteness, the relative permittivity of the rhodamine mixture was fixed at $2 - 0.02i$. By means of the forward Bruggeman homogenization formalism,[32] the relative permittivity scalars for the zirconium oxide CSTF — whose nanowires are impregnated with silver nanoparticles and whose inter-nanowire regions are filled with a rhodamine mixture — were then estimated to be $\varepsilon_a = 3.135 - 0.002i$, $\varepsilon_b = 2.865 - 0.012i$, and $\varepsilon_c = 3.321 + 0.005i$.

Notice that the particular choices of the rise angle χ, volume fraction f, and concentration of silver nanoparticles result in the imaginary parts of $\varepsilon_{a,b,c}$ having different signs, from which it may be inferred that planewave propagation in different directions in the CSTF can be simultaneously attenuative and amplifying.[2] Also, in order to highlight the reflectance/transmission properties of the CSTF, the gain properties of the rhodamine mixture are held constant across the free-wavelength range 550 nm $< \lambda_0 <$ 800 nm. If known, the frequency dependence of constitutive parameters can be easily accommodated in our calculations.[20,27]

3 Reflection–transmission investigation

Suppose that the CSTF occupies the region $0 < z < L$, the regions $z < 0$ and $z > L$ being vacuous. An incident plane wave of arbitrary polarization state illuminates the face $z = 0$ of the CSTF, with angle of incidence θ with respect to the z axis and angle of incidence ψ with respect to the x axis in the xy plane, as illustrated schematically in Fig. 2. A 4×4-matrix–based procedure to calculate the remittances of the CSTF is explained elsewhere[20] in detail. Using this procedure, we calculated the four circular reflectances ($R_{RR,RL,LR,LL}$) and the four circular transmittances ($T_{RR,RL,LR,LL}$) as functions of $\lambda_0 \in (550, 800)$ nm for wide ranges of the angles of incidence θ and ψ. Here, R_{LR} is the fraction of the incident power reflected via a *L*eft-circularly polarized plane wave when the incident plane wave is *R*ight-circularly polarized, and so on.

If the CSTF were to be wholly dissipative (i.e., in the absence of amplification), then the principle of conservation of energy would require the inequalities

$$\left.\begin{array}{l} R_{LL} + R_{RL} + T_{LL} + T_{RL} < 1 \\ R_{LR} + R_{RR} + T_{LR} + T_{RR} < 1 \end{array}\right\} \tag{7}$$

to be satisfied. Conversely, if the CSTF were wholly active then the inequalities

$$\left.\begin{array}{l} R_{LL} + R_{RL} + T_{LL} + T_{RL} > 1 \\ R_{LR} + R_{RR} + T_{LR} + T_{RR} > 1 \end{array}\right\} \tag{8}$$

would apply.

For illustrative results, the CSTF thickness was taken to be $L = 2\Omega N$ with structural half-period $\Omega = 200$ nm and N being a positive integer. The structural-handedness parameter was set at $h = +1$.

We begin with $N = 25$ and azimuthal angle $\psi = 0°$. The remittance sums $R_{LL} + R_{RL}$ and $T_{LL} + T_{RL}$ for LCP incident light, and $R_{LR} + R_{RR}$ and $T_{LR} + T_{RR}$ for RCP incident light, are plotted against λ_0 in Fig. 3 for the polar angle $\theta \in \{5\text{ deg}, 30\text{ deg}, 60\text{ deg}\}$. The plot of $R_{LR} + R_{RR}$ for $\theta = 5$ deg exhibits a distinct window $670\,\text{nm} \lessapprox \lambda_0 \lessapprox 732\,\text{nm}$ of high reflectance, which is matched by a distinct window of generally very low $T_{LR} + T_{RR}$ (albeit there is a substantial spike in $T_{LR} + T_{RR}$ at the shortest wavelength edge of the spectral window). As the polar angle θ increases, the spectral regime of high $R_{LR} + R_{RR}$ and very low $T_{LR} + T_{RR}$ blue shifts substantially. Specifically, when $\theta = 60$ deg the spectral regime for high $R_{LR} + R_{RR}$ and very low $T_{LR} + T_{RR}$ is $588\,\text{nm} \lessapprox \lambda_0 \lessapprox 648\,\text{nm}$. This circular Bragg phenomenon[36] — characterized by a spectral regime of high reflectance and low transmittance — is not apparent in the plots of $R_{LL} + R_{RL}$ and $T_{LL} + T_{RL}$ for LCP incident light.

Most significantly, within the circular Bragg regime there a exists spectral regime for which $R_{LR} + R_{RR} > 1$. For example, $R_{LR} + R_{RR} > 1$ for $684\,\text{nm} \lessapprox \lambda_0 \lessapprox 696\,\text{nm}$ when $\theta = 5$ deg. Thus, not only does the CSTF function as a good circular Bragg mirror for RCP incident light, but for a substantial proportion of the circular Bragg regime it functions as a circular Bragg supermirror since the reflected light is amplified in this portion of the circular Bragg regime.

The remittance sums $R_{LL}+R_{RL}+T_{LL}+T_{RL}$ for LCP incident light and $R_{LR}+R_{RR}+T_{LR}+T_{RR}$ for RCP incident light are also plotted in Fig. 3 as functions of λ_0 for $\theta \in \{5\text{ deg}, 30\text{ deg}, 60\text{ deg}\}$. For all values of λ_0, the remittance sum $R_{LL} + R_{RL} + T_{LL} + T_{RL} > 1$. Thus, incident LCP light is amplified inside the CSTF. The situation is mixed for incident RCP light. The remittance sum $R_{LR} + R_{RR} + T_{LR} + T_{RR}$ exceeds unity for most values of λ_0, but is less than unity on the long-wavelength side of the circular Bragg regime Thus, incident RCP light is amplified inside the CSTF at wavelengths shorter than those of the circular Bragg regime, but attenuated at wavelengths in the vicinity of the long-wavelength limit of the circular Bragg regime.

In order to further highlight the competing effects of gain and loss, we considered the CSTF to be made only of zirconium oxide and infiltrated by air. Then, as both silver nanoparticles and the rhodamine mixture are absent, the CSTF is wholly lossless (and wholly inactive). Thus, in Fig. 4 the remittance sums $R_{LL} + R_{RL}$ and $T_{LL} + T_{RL}$ for LCP incident light, and $R_{LR} + R_{RR}$ and $T_{LR} + T_{RR}$ for RCP incident light, are plotted against λ_0 for the CSTF specified by $\varepsilon_a = 3.135$, $\varepsilon_b = 2.865$, and $\varepsilon_c = 3.321$. As in Fig. 3, $\theta \in \{5\text{ deg}, 30\text{ deg}, 60\text{ deg}\}$, $\psi = 0$ deg, and $N = 25$. The circular Bragg phenomenon manifests itself as a window of high reflectance sum $R_{LR} + R_{RR}$ and low transmittance sum $T_{LR} + T_{RR}$ which is blue shifted as the angle θ increases. And this phenomenon is not observed for LCP incident light. Most significantly, all the remittance sums presented in Fig. 4 are less than or equal to unity for all values of λ_0, which is in stark contrast to the case presented in Fig. 3 wherein the active nature of the rhodamine mixture leads to remittance sums that exceed unity. Plots of the reflectance–transmittance sums $R_{LL} + R_{RL} + T_{LL} + T_{RL}$ and

$R_{LR} + R_{RR} + T_{LR} + T_{RR}$ are not presented in Fig. 4 as these quantities are both equal to unity, for all values of λ_0.

By varying the azimuthal angle ψ, qualitatively similar results to those presented in Fig. 3 for $\psi = 0$ deg emerge. For a representative example, in Fig. 5 plots analogous to those of Fig. 3 but for $\psi = 90$ deg are presented. As in Fig. 3, the Bragg phenomenon is clearly observable in the plots of the reflectance sum $R_{LR} + R_{RR}$ and transmittance sum $T_{LR} + T_{RR}$ for RCP incident light, but there is no Bragg phenomenon in the case of LCP incident light. Furthermore, the circular Bragg regime substantially blue shifts as the polar angle θ increases. Also, at $\psi = 90$ deg the CSTF functions as a circular Bragg supermirror for incident RCP light. To wit, $R_{LR} + R_{RR} > 1$ for $682\,\text{nm} \lessapprox \lambda_0 \lessapprox 694\,\text{nm}$ when $\theta = 5$ deg. And, similarly to the case for $\psi = 0$ deg, when $\psi = 90$ deg LCP incident light is amplified by the CSTF, and so largely is RCP incident light with the exception of wavelengths in the vicinity of the long-wavelength limit of the circular Bragg regime.

The spectral regime, within the circular Bragg regime, in which the CSTF functions as a circular Bragg supermirror may be enlarged by increasing the thickness of the CSTF. In Fig. 6 plots analogous to those in Fig. 3 but computed with $N = 50$ are presented. The circular-Bragg-supermirror regime, apparent from the plots of the reflectance sum $R_{LR} + R_{RR}$ in Fig. 6, extends over the range $676\,\text{nm} \lessapprox \lambda_0 \lessapprox 700\,\text{nm}$ when $\theta = 5$ deg, for example, which is slightly larger than is the case observed in Fig. 3. Furthermore, the average magnitude of $R_{LR} + R_{RR}$ in Fig. 6 over the circular-Bragg-supermirror regime is larger than the corresponding average magnitude in Fig. 3. The other remittance-sum plots in Fig. 6 are qualitatively similar to those in Fig. 3 but with the plots in Fig. 6 generally exhibiting higher-frequency Fabry–Perot oscillations than those in Fig. 3.

4 Closing remarks

Our numerical study has revealed that a CSTF infiltrated with an active material simultaneously amplifies left-circularly polarized incident light and attenuates right-circularly-polarized incident light, or vice versa, depending upon the CSTF's structural handedness. This polarization-state-dependent attenuation and amplification phenomenon is sensitive to the direction of incidence and the thickness of the CSTF. Furthermore, the presence of both dissipative and active materials allows the high reflectance to exceed unity across a substantial proportion of the circular Bragg spectral regime for incident light of one circular polarization state but not of the other circular polarization state. Hence, the CSTF functions as a circular Bragg supermirror for one, and only one, circular polarization state. It is notable that spectral regime in which the CSTF functions as a circular Bragg supermirror here is much larger than reported for other configurations of CSTFs involving active materials. For example, if a CSTF is infiltrated with a Raman–active liquid then the CSTF functions as a supermirror only for a very narrow spectral range (i.e, approximately 0.1 nm), albeit this very narrow spectral range can be positioned anywhere within the circular Bragg regime.[37] Also, if the CSTF is made entirely from an active material then it can function as a circular Bragg supermirror across two very narrow spectral ranges, at the two edges of the circular Bragg regime.[38]

Acknowledgment. AL is grateful to the Charles Godfrey Binder Endowment at Penn State for ongoing support of his research.

References

1 R. M. Walser, Metamaterials: An introduction. In: W. S. Weiglhofer and A. Lakhtakia (Eds.), *Introduction to Complex Mediums for Optics and Electromagnetics*, pp. 295–316, SPIE Press, Bellingham, WA, USA (2003).

2 T. G. Mackay and A. Lakhtakia, Dynamically controllable anisotropic metamaterials with simultaneous attenuation and amplification, *Phys. Rev. A* **92**, 053847 (2015).

3 A. Cerjan and S. Fan, Achieving arbitrary control over pairs of polarization states using complex birefringent metamaterials, *Phys. Rev. Lett.* **118**, 253902 (2017).

4 T. G. Mackay and A. Lakhtakia, Simultaneous amplification and attenuation in isotropic chiral materials, *J. Opt. (UK)* **18**, 055104 (2016).

5 S. Wuestner, A. Pusch, K.L. Tsakmakidis, J.M. Hamm, and O. Hess, Overcoming losses with gain in a negative refractive index metamaterial, *Phys. Rev. Lett.* **105**, 127401 (2010).

6 Z.-G. Dong, H. Liu, T. Li, Z.-H. Zhu, S.-M. Wang, J.-X. Cao, S.-N. Zhu, and X. Zhang, Optical loss compensation in a bulk left-handed metamaterial by the gain in quantum dots, *Appl. Phys. Lett.* **96**, 044104 (2010).

7 G. Strangi, A. De Luca, S. Ravaine, M. Ferrie, and R. Bartolino, Gain induced optical transparency in metamaterials, *Appl. Phys. Lett.* **98**, 251912 (2011).

8 W. Xu, W. J. Padilla, and S. Sonkusale, Loss compensation in metamaterials through embedding of active transistor based negative differential resistance circuits, *Opt. Exp.* **20**, 22406–22411 (2012).

9 L. Sun, X. Yang, and J. Gao, Loss-compensated broadband epsilon-near-zero metamaterials with gain media, *Appl. Phys. Lett.* **103**, 201109 (2013).

10 T. G. Mackay and A. Lakhtakia, Polarization-state-dependent attenuation and amplification in a columnar thin film, *J. Opt. (UK)* **19**, 12LT01 (2017). Erratum **20**, 019501 (2018).

11 V. Vepachedu, T. G. Mackay, and A. Lakhtakia, Bragg supermirror with polarization-dependent amplification of reflected light, *Opt. Commun.* **425**, 58–63 (2018).

12 W. H. Bragg and W. L. Bragg, The reflexion of X-rays by crystals, *Proc. R. Soc. Lond. A* **88**, 428–438 (1913).

13 W. H. Bragg, The intensity of reflexion of X rays by crystals, *Phil. Mag. (Ser. 6)* **27**, 881–899 (1914).

14 E. Reusch, Untersuchung über Glimmercombinationen, *Ann. Phys. Chem. Lpz.* **138**, 628–638 (1869).

15 J. C. Bose, On the rotation of plane of polarisation of electric waves by a twisted structure, *Proc. R. Soc. Lond.* **63**, 146–152 (1898).

16 N. O. Young and J. Kowal, Optically active fluorite films, *Nature* **183**, 104–105 (1959).

17 E. F. Dawson and N. O. Young, Helical Kerr cells, *J. Opt. Soc. Am.* **50**, 170–171 (1960).

18 G. Joly and N. Isaert, Quelques champs électromagnétiques dans les piles de Reusch IV. Domaines multiples de réflexion sélective, *J. Opt. (Paris)* **17**, 211–221 (1986).

19 L. De Silva, I. Hodgkinson, P. Murray, Q. H. Wu, M. Arnold, and J. Leader, Natural and nanoengineered chiral reflectors: structural color of Manuka beetles and titania coatings, *Electromagnetics* **25**, 391–408 (2005).

20 A. Lakhtakia and R. Messier, *Sculptured Thin Films: Nanoengineered Morphology and Optics*, SPIE Press, Bellingham, WA, USA (2005).

21 J. K. Gansel, M. Thiel, M. S. Rill, M. Decker, K. Bade, V. Saile, G. von Freymann, S. Linden, and M. Wegener, Gold helix photonic metamaterial as broadband circular polarizer, *Science* **325**, 1513–1515 (2009).
22 J. Kaschke, J. K. Gansel, and M. Wegener, On metamaterial circular polarizers based on metal N-helices, *Opt. Expr.* **20**, 26012–26020 (2012).
23 V. C. Venugopal, Three-dimensional periodic chiral sculptured thin films, *J. Nanophotonics* **7**, 073502 (2013).
24 H.-H. Huang and Y.-C. Hung, Designs of helix metamaterials for broadband and high-transmission polarization rotation, *IEEE Photon. J.* **6**, 4600207 (2014).
25 A. S. Chadha, D. Zhao, and W. Zhou, Comparative study of metallic and dielectric helix photonic metamaterial, *Opt. Mater. Expr.* **4**, 2460–2467 (2014).
26 S. Agarwal and Y. K. Prajapati, Broadband and polarization-insensitive helix metamaterial absorber using graphene for terahertz region, *Appl. Phys. A* **122**, 561 (2016).
27 S. Erten, M. Faryad, and A. Lakhtakia, Multiple surface-plasmon-polariton waves guided by a chiral sculptured thin film grown on a metallic grating, *J. Opt. Soc. Am. B* **34**, 1937–1945 (2017).
28 I. J. Hodgkinson and Q. h. Wu, *Birefringent Thin Films and Polarizing Elements*, World Scientific, Singapore (1997).
29 D. A. G. Bruggeman, Berechnung verschiedener physikalischer Konstanten von heterogenen Substanzen, I. Dielektrizitätskonstanten und Leitfähigkeiten der Mischkörper aus isotropen Substanzen, *Ann. Phys. Chem. Lpz.* **24**, 636–679 (1935).
30 L. Ward, *The Optical Constants of Bulk Materials and Films, 2nd Edition*, IOP Publishing, Bristol, UK (1994).
31 T. G. Mackay and A. Lakhtakia, *Modern Analytical Electromagnetic Homogenization*, IOP Publishing, Bristol, UK (2015).
32 T. G. Mackay and A. Lakhtakia, Determination of constitutive and morphological parameters of columnar thin films by inverse homogenization, *J. Nanophoton.* **4**, 041535 (2010).
33 I. J. Hodgkinson, Q. h. Wu, and J. Hazel, Empirical equations for the principal refractive indices and column angle of obliquely-deposited films of tantalum oxide, titanium oxide and zirconium oxide, *Appl. Opt.* **37**, 2653–2659 (1998).
34 J.-B. Biot and F. Arago, Mèmoire sur les affinités des corps pour la lumière et particulièrement sur les forces réfringentes des différents gaz, *Mém. Inst. Fr.* **7**, 301–385 (1806).
35 W. Cai and V. M. Shalaev, *Optical Metamaterials*, Springer, New York, NY, USA (2010).
36 M. Faryad and A. Lakhtakia, The circular Bragg phenomenon, *Adv. Opt. Photon.* **6**, 225–292 (2014).
37 A. Lakhtakia and S. A. Ramakrishna, Narrowband enhancement of the circular Bragg phenomenon by stimulated Raman scattering, *J. Opt. (UK)* **12**, 085101 (2010). Erratum **12**, 089802 (2010).
38 A. Lakhtakia and J. Xu, Planewave remittances of an axially excited chiral sculptured thin film with gain, *Optik* **118**, 94–99 (2007).

Biographies

Tom G. Mackay is a reader in the School of Mathematics at the University of Edinburgh and an adjunct professor in the Department of Engineering Science and Mechanics at the Pennsylvania State University. His current research interests include homogenization, complex materials, and sculptured thin films. He became a Fellow of SPIE in 2010.

Akhlesh Lakhtakia is Evan Pugh University Professor and Charles Godfrey Binder Professor at the Pennsylvania State University. His current research interests include surface multiplasmonics, solar cells, sculptured thin films, mimumes, multicontrollability, bioreplication, and forensic science. He has been elected a fellow of Optical Society of America, SPIE, Institute of Physics, American Association for the Advancement of Science, American Physical Society, Institute of Electrical and Electronics Engineers, Royal Society of Chemistry, and Royal Society of Arts. He received the 2010 SPIE Technical Achievement Award and the 2016 Walston Chubb Award for Innovation.

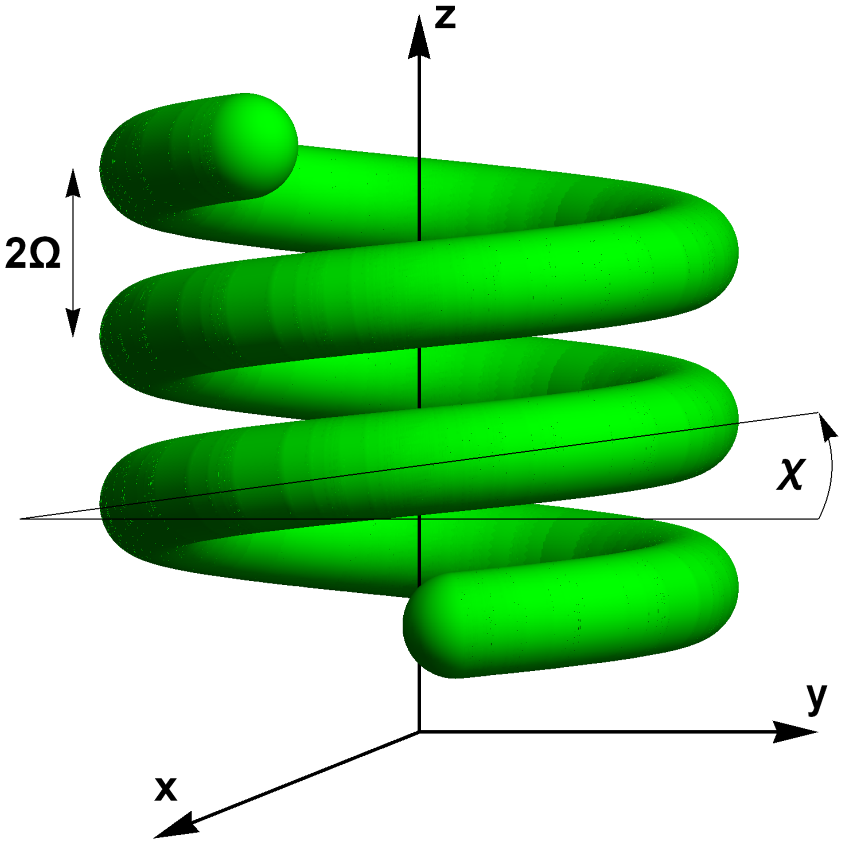

Fig 1 Schematic representation of a helical nanowire in a CSTF, with the structural period 2Ω and the rise angle χ indicated.

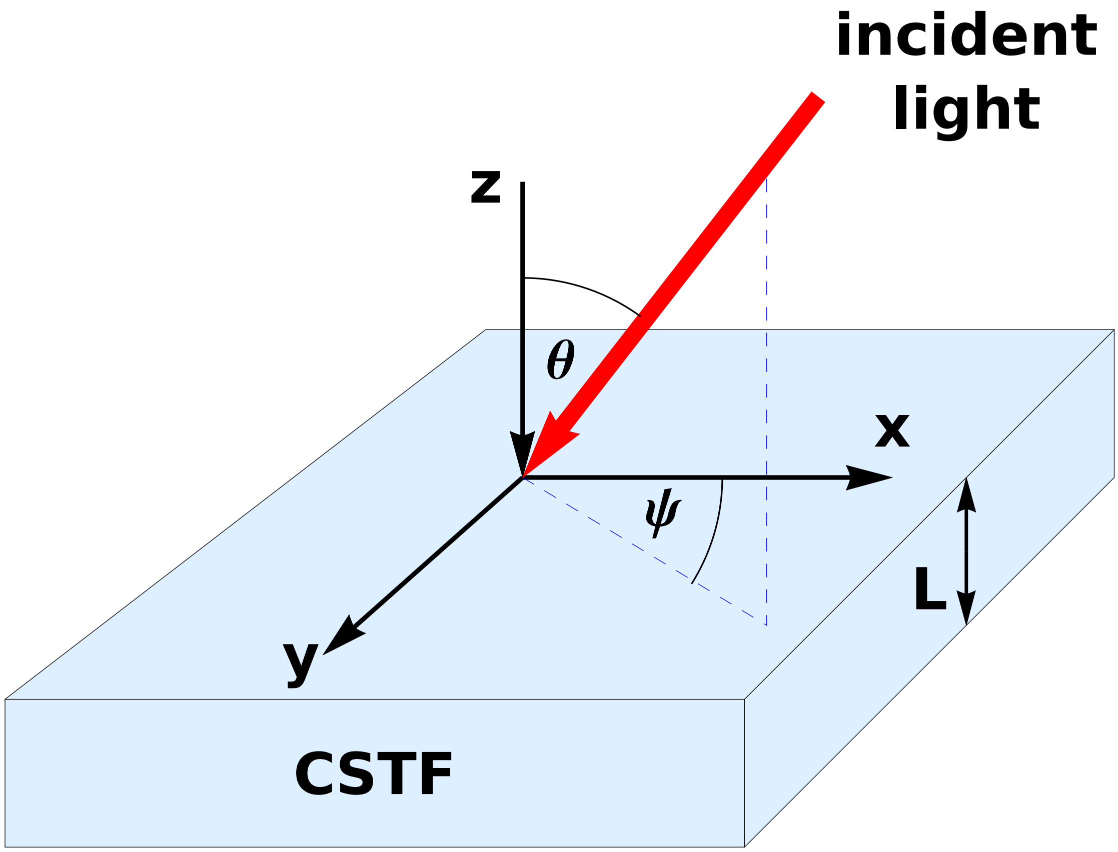

Fig 2 Schematic representation of the reflection–transmission problem for a CSTF of thickness L, illustrating the angles of incidence ψ and θ.

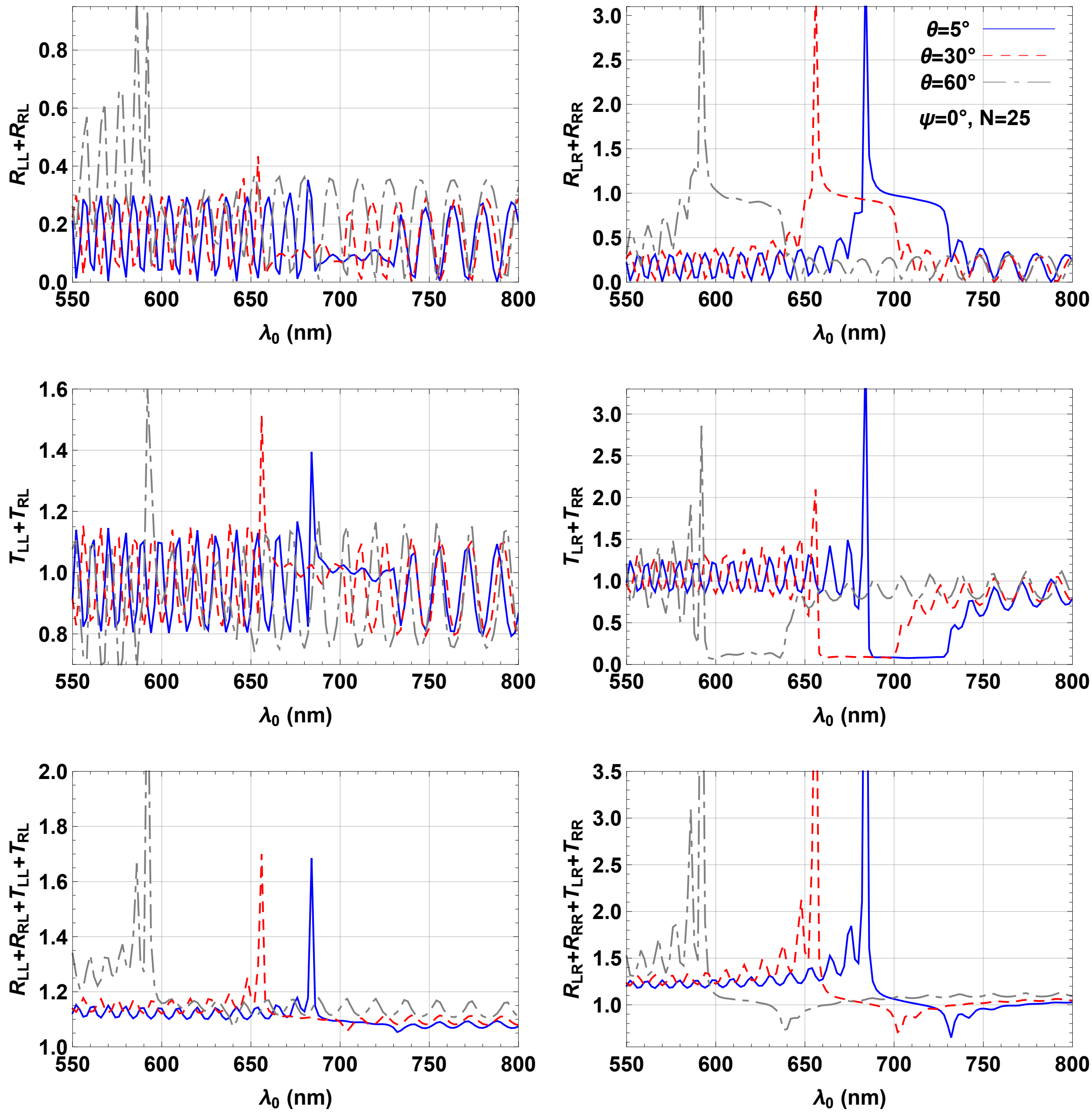

Fig 3 Reflectance sums $R_{LL}+R_{RL}$ and $R_{LR}+R_{RR}$, transmittance sums $T_{LL}+T_{RL}$ and $T_{LR}+T_{RR}$, and reflectance–transmittance sums $R_{LL}+R_{RL}+T_{LL}+T_{RL}$ and $R_{LR}+R_{RR}+T_{LR}+T_{RR}$ plotted against $\lambda_0 \in (550, 800)$ nm for $\theta \in \{5 \text{ deg}, 30 \text{ deg}, 60 \text{ deg}\}$ and $\psi = 0$ deg, with $N = 25$.

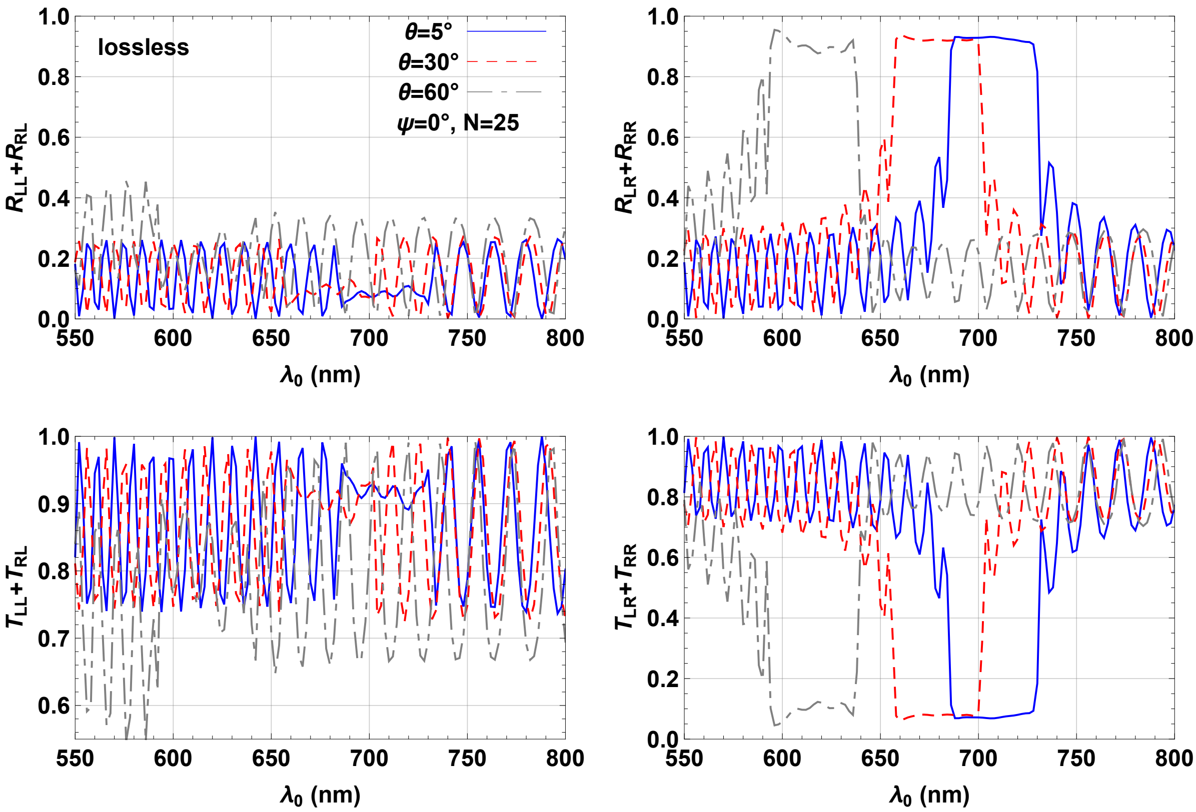

Fig 4 As Fig. 3 but when the silver nanoparticles and the rhodamine mixture are absent, so that the CSTF is specified by $\varepsilon_a = 3.135$, $\varepsilon_b = 2.865$, and $\varepsilon_c = 3.321$. Plots of the reflectance–transmittance sums $R_{LL} + R_{RL} + T_{LL} + T_{RL}$ and $R_{LR} + R_{RR} + T_{LR} + T_{RR}$ are not presented as these quantities are both equal to unity, for all values of λ_0.

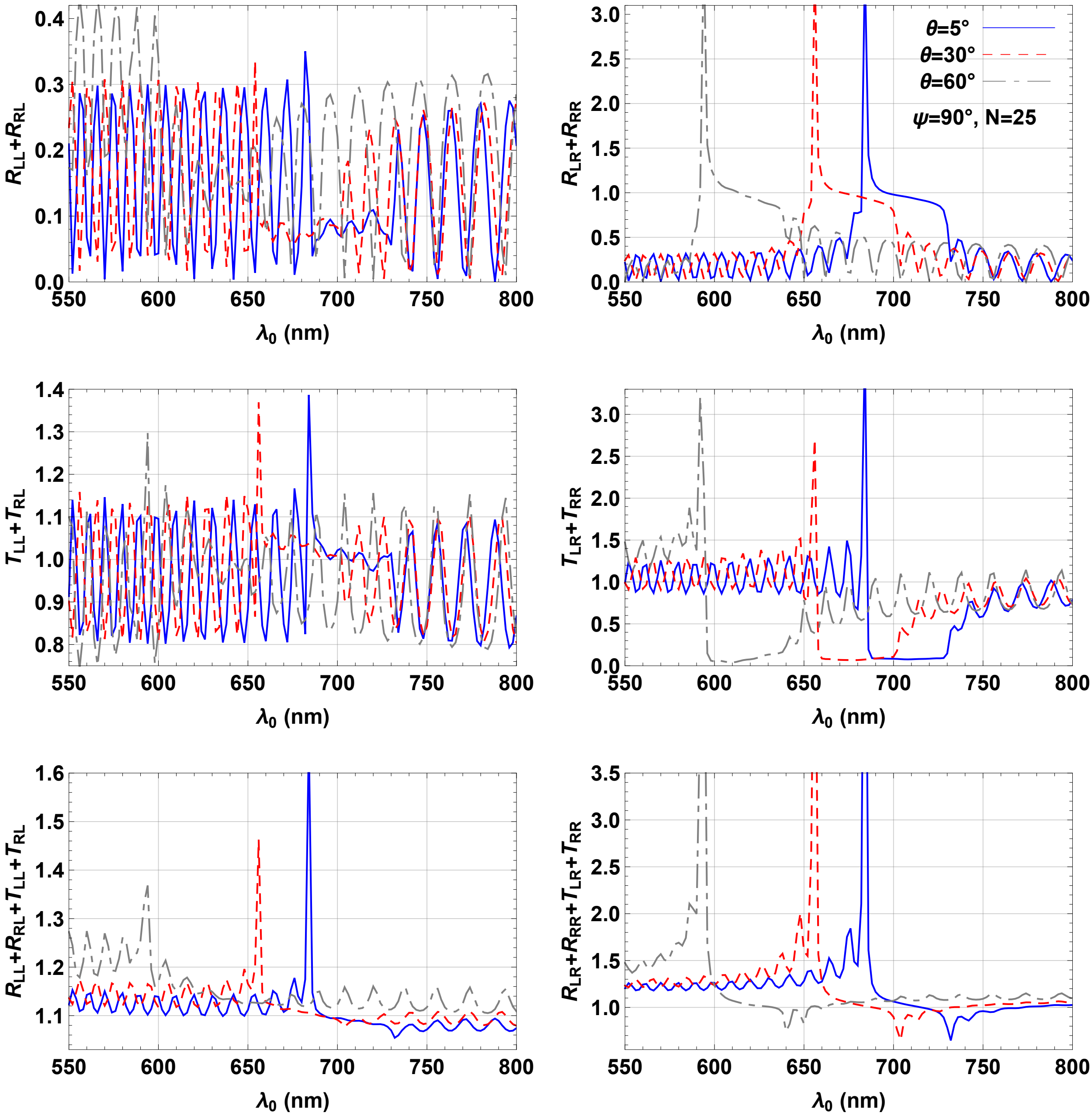

Fig 5 As Fig. 3 but for $\psi = 90$ deg.

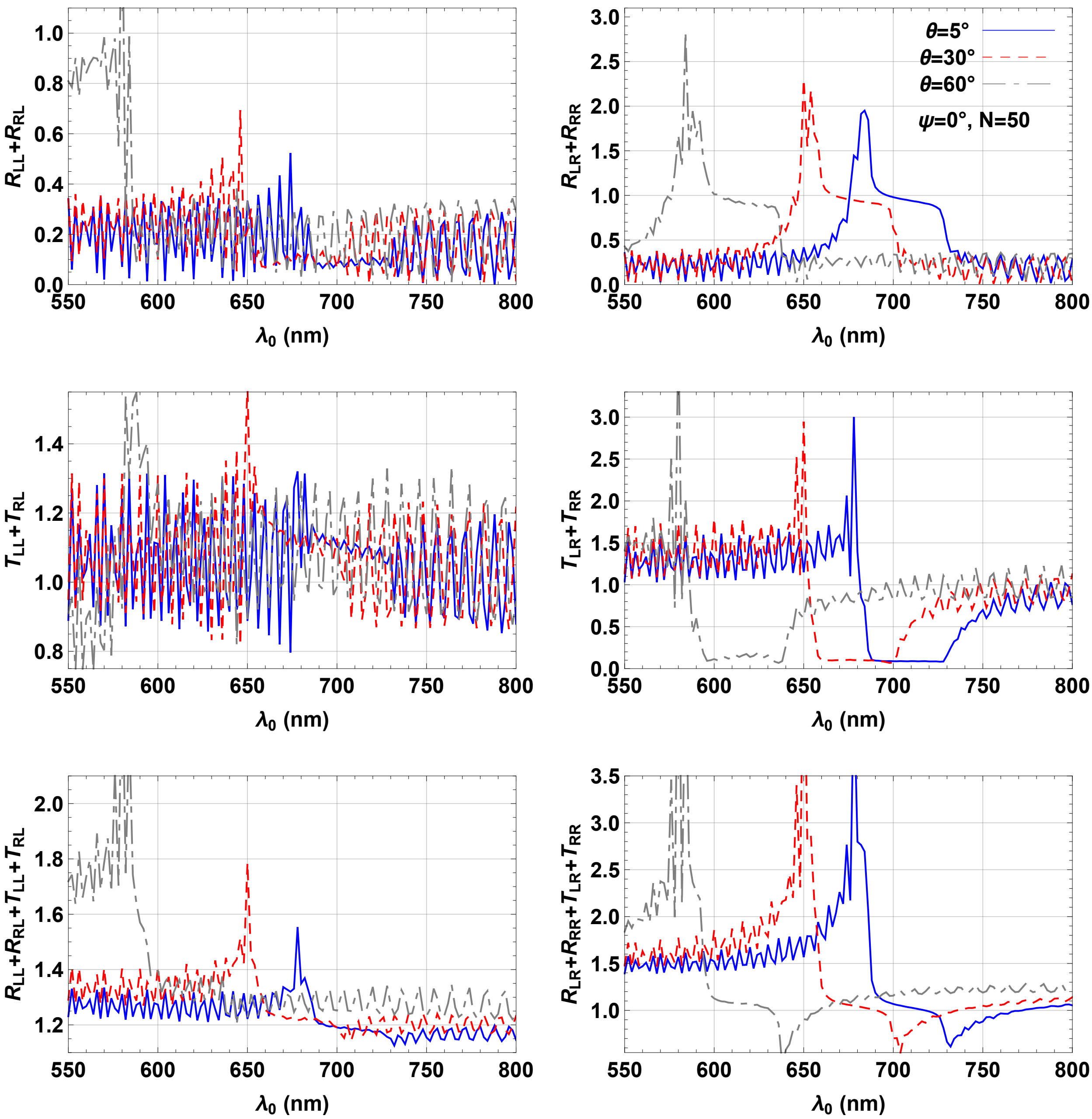

Fig 6 As Fig. 3 but for $N = 50$.